

Rule-based guidance for flight vehicle flocking

Bill Crowther¹, School of Engineering, University of Manchester, UK

Copyright Bill Crowther, September 2002

Abstract

Within nature, mobile organisms often exhibit a form of emergent behaviour known as flocking. Flocking is adaptive because for a given population density, the information processing required for collision avoidance is minimized. Within human activities, the problem of increasing civil air traffic is leading to consideration of decentralized traffic management methodologies, such as Free Flight. On the other hand, for military flight vehicles, safe operation of flight vehicles at high air space densities is seen as an opportunity. The present paper considers the use of guidance based on flocking rules to support the management of flight vehicles in situations of high airspace density. Three elemental flocking schemes are identified based on guidance tasks and a simple analytical framework is developed that allows insight into the fundamental flocking behavior for all three schemes. Flight vehicles are modeled as point masses moving with constant speed in the horizontal plane. CCA non-dimensional approach is used throughout to provide generality. The proposed flocking algorithm is implemented within Matlab and numerical simulation results are used to validate analytical predictions of steady state flock size and entropy. Results show that a simple parameter based on the ratio of rule weights is sufficient to predict flock behaviour.

Nomenclature

A	alignment vector
B	cohesion vector
F	flocking parameter
g	acceleration due to gravity (m/s ²)
L	lift force (N)
m	number of boids
n	load factor
r	non-dimensional turn radius
R	Turn radius (m)
R_o	flock length scale (m)
t	dimensional time (s)
T_o	flock time scale (s)
V_∞	flight vehicle velocity (m/s)
W	flight vehicle weight (kg)
W_α	alignment rule weight
W_β	cohesion rule weight
x	displacement (m)
X	position vector (m)

¹ Lecturer, School of Engineering, University of Manchester, Manchester M13 7LP, UK. www.billcrowther.info

\dot{x}	velocity in x direction (m)
y	displacement (m)
\dot{y}	velocity y direction (m)
α	alignment angle (radians)
β	cohesion angle (radians)
ϕ	bank angle (radians)
σ_x	non-dimensional standard deviation of position (flock size)
σ_v	non-dimensional standard deviation of velocity (flock entropy)
τ	non-dimensional time
ψ	heading angle (radians)
$\dot{\psi}$	turn rate (radians/s)

Subscripts

i	individual boid index
j	flock boid index
α	alignment
β	cohesion

List of Figure

Figure 1 *Schematic representation of the alignment and cohesion rules for flocking*

Figure 2 *Definition of three different flocking schemes*

Figure 3 *Aircraft performing a steady, banked turn in the horizontal plane*

Figure 4 *Angle, position and vector definitions for a flocking boid*

Figure 5 *Schematic of the three fundamental flocking modes*

Figure 6 *Logic flow diagram for flocking algorithm implementation*

Figure 7 *Effect of guidance interval on flock entropy time history for an alignment weighting of 4, cohesion weighting = 0, scheme A flocking. Guidance interval independence is achieved for $\tau_{\text{guidance}} < 0.1$.*

Figure 8 *Flock size time histories for varying cruise speed, fixed rule weightings, scheme B flocking. The collapse of the data demonstrates validity of the velocity scaling used.*

Figure 9 *Flock size time histories for varying cohesion rule weight, scheme B flocking.*

Figure 10 *Steady state flock size as a function of cohesion rule weighting, scheme B flocking. A strong correlation between numerical and analytical results is demonstrated.*

Figure 11 *Steady state flock size and flock entropy contours as a function of alignment and cohesion rule weights for flocking schemes A, B and C. Note that all three flocking schemes show qualitatively similar results. From this figure, it can be concluded that the ratio of alignment to cohesion rule weights is the fundamental parameter determining flocking steady state behaviour.*

Figure 12 *Steady state flock size and entropy as a function of the ratio of alignment to cohesion rule weights, scheme A flocking.*

Figure 13 *Schematic representation of figure 12 correlating flock modes with different flocking parameter zones.*

Figure 14 *Flock size and entropy time histories for varying flocking parameter, scheme A flocking*

Figure 15 *Boid trajectories for varying values of flocking parameter, scheme A flocking*

Figure 16 *Flock size and entropy time histories for varying flocking parameter, scheme B flocking*

Figure 17 *Boid trajectories for varying values of flocking parameter, scheme B flocking*

I. Introduction

Continual growth in global air traffic is putting increasing pressure on traditional airspace management capabilities, which are currently based on fixed geographical zones and fixed flight corridors managed by individual air traffic control centres. A proposed solution to this problem is the Free Flight system (1)(2), in which ground-based software networked across geographical zones is used to assign individual, optimised flight corridors for each participating aircraft. Furthermore, participating aircraft have greater autonomy, with aircraft being able to negotiate with the ground based system and with other aircraft to reduce fuel burn or flight time without compromising safety. It is also expected that aircraft could manage spatial conflict scenarios between two aircraft directly without ground intervention (3)(4). However, at very high traffic densities it may be necessary to resolve conflicts with an increasing number of aircraft simultaneously (5)(6), which poses a very high computational cost and increased risk.

Whilst crowded skies are an impediment to civil aviation, there are a number of military scenarios where high airspace density is advantageous, particularly with the increasing use of unmanned air vehicles. For example, sensors can be distributed across multiple vehicles to increase sensor aperture and secure, high bandwidth, point-to-point communication networks can be created without the use of satellite uplinks. In addition, multiple vehicles, if sufficiently organised, can be used to optimise search, identify and respond missions (7).

In nature, aggregations of large numbers of mobile organisms are also faced with the problem of organising themselves efficiently. This selective pressure has led to the evolution of behaviour such as herding of land animals (8), flocking of birds (9), swarming of insects, and schooling of fish (10)(11). The main motivation for synchronising the dynamics in such groups is that it minimises the information processing and actuation energy required for collision avoidance. Collective motion also has other benefits in terms of confusing predators and social bonding.

More generally, emergent behaviour is often observed in multi-agent systems (12). Within this context, agents can be birds within a flock, nodes within a communications or power distribution network, or virtual traders in a stock market. In some cases, emergent phenomena are undesirable; for instance the spontaneous collapse of distribution networks, or increased market volatility.

Within the present work, a flock may be defined as a system of mobile autonomous agents exhibiting the essential behaviors of spatial and velocity coherence. The overall control of the flock is decentralized in that its global motion is controlled by rules that operate at the local level.

A swarm behaves in a similar way to a flock; however, its velocity coherence is typically much lower. Formation flight, on the other hand, is quite distinct from flocking. In a formation, vehicles are generally arranged according to fixed spatial

relationships and the behaviour of the group is typically controlled by rules operating at the global level. Formation flight has recently been studied for both groups of aircraft (13)(14)(15) and constellations of satellites (16).

Many previous studies have demonstrated that visually interesting flocking behaviour can be obtained by the application of local rules to mobile agents, the first well-documented example being by Reynolds (17). The main application for this work has been in the entertainment industry, providing an efficient means of generating computer animations of natural-looking behaviours for film, television and computer games.

Emergent behaviour in the collective motion of particle systems has been studied by a number of authors. In particular, Shimoyama et al (18) use non-dimensional time and length scales to categorize the types of behaviour obtained for a number of simulated individuals, and the conditions for transition between phases. Other studies have used a statistical physics approach to predict both phase transitions and the dynamics of information exchange within the flock (19)(20)(21).

The aim of the present work is to provide a sound theoretical basis for the practical application of flocking techniques to flight vehicle airspace management. The work is distinct from other more general flocking studies in that the problem is formulated firmly within a flight vehicle guidance and control framework. It is shown that the fundamental type of flocking behaviour can be predicted based on a small number of non-dimensional parameters. The work builds upon a previous study that qualitatively investigated the behaviour of a flock of simulated unmanned air vehicles (22).

In the following, section II describes the fundamentals of flight vehicle flocking and derives the key equations modelling the behaviour of an individual within a flock. Steady state solutions of these equations are then obtained to identify characteristic flock behaviours or modes. The numerical approach used to obtain transient solutions of the flocking equations is described in section III with simulation results described in section IV. Conclusions are drawn in section V and further work described in section VI.

II. Theory

A. Rules of flocking

Three general approaches to the problem of path planning for mobile agents can be identified (23). These are cell decomposition methods, roadmap methods and artificial potential field methods. The former two methods are computationally intensive and most appropriate for defining complete paths for small numbers of individuals in an environment cluttered with obstacles. On the other hand, the simpler potential field method (24) can only predict the local direction in which an agent should move, however it is amenable to inclusion of large numbers of mobile individuals. Most previous flocking studies have modelled flocking behaviour using a potential field method, expressed in the form of a number of flocking rules. The present study also adopts this approach.

The two primary rules of flocking behaviour are illustrated in figure 1. The alignment rule (figure 1a) represents the urge to fly in the same direction as the local flock (alignment centroid), whereas the cohesion rule (figure 1b) represents the urge to fly towards the local flock centre of gravity (cohesion centroid). Each rule has a degree of

locality illustrated by the light coloured circle surrounding the flight vehicle, or boid, of interest. (Within flocking terminology, boid is a general term used for an individual agent within a flock. It is short for bird-android). The resultant motion of a given boid is determined by the weighted vector sum of the two rule outputs.

For simplicity in the present work, the degree of locality for each rule is infinite. This means that the alignment and cohesion centroids can be calculated globally, reducing the computational overhead.

B. Flocking schemes

For the purposes of the present work, three different types of flocking scheme are identified, figure 2. In scheme A, boids fly as a flock along a predefined alignment vector. This scheme can be used as a simple means of controlling the direction of travel of the flock. In scheme B, boids fly as a flock around a predefined cohesion centroid. This scheme can be used as a means of flock station-keeping around a fixed point for observation or air traffic control needs. Finally, with scheme C, boids fly as a flock with no predefined alignment vector or cohesion centroid (free flocking). Scheme C is often used for computer animation purposes.

C. Implementation

1. Aircraft turning flight

The way in which flocking rules are implemented depends on the dynamics and control of the system at hand. In the present work for application to aircraft, the system dynamics are represented by a point mass moving at constant speed in the horizontal plane, and control is via acceleration in the horizontal plane normal to the direction of motion. This corresponds to aircraft flying at constant speed using bank to turn.

An aircraft performing a level turn is shown in figure 3. Using Newton's Second Law for angular motion it can be shown (25) that the turn rate, $\dot{\psi}$, is given by

$$\dot{\psi}_i = \frac{g\sqrt{n^2 - 1}}{V_\infty} \quad (\text{Equation 1})$$

and the turn radius, R , by

$$R = \frac{V_\infty^2}{g\sqrt{n^2 - 1}} \quad (\text{Equation 2})$$

where n is the load factor, defined as

$$n = \frac{L}{W} = \frac{1}{\cos \phi} \quad (\text{Equation 3})$$

and g is the acceleration due to gravity.

The linear velocity of the aircraft is given by

$$\dot{X} = V_\infty \cos \psi \quad (\text{Equation 4})$$

$$\dot{Y} = V_\infty \sin \psi \quad (\text{Equation 5})$$

2. Flock dynamics

In this section, guidance information in the form of an expression for the demand load factor, n , for a given boid is derived from the flocking rules. This will then be substituted into equation 1 to give a general equation for the flock dynamics.

Figure 4 defines the angles, positions and vectors for a boid i within a flock of m similar boids. Boid i is located at \mathbf{X}_i and has velocity vector \mathbf{V}_i along a heading angle ψ_i . The flock cohesion centroid q is located at \mathbf{X}_q with the boid cohesion vector \mathbf{B}_i given by $\mathbf{B}_i = \mathbf{X}_q - \mathbf{X}_i$, orientated at an angle β_i . The alignment vector, common to all boids, is \mathbf{A} and is orientated at an angle α .

For the general case of m boids, equation 1 is written

$$\psi_i = \frac{g\sqrt{n_i^2 - 1}}{V_\infty} \quad i = 1:m \quad (\text{Equation 6})$$

Within the present work, guidance information for a given boid is based on the heading angle errors for each of the rules. These are defined as follows:

$$\psi_{\alpha i} = \alpha - \psi_i, \quad -\pi < \psi_{\alpha i} < \pi \quad (\text{Equation 7})$$

$$\psi_{\beta i} = \beta_i - \psi_i, \quad -\pi < \psi_{\beta i} < \pi \quad (\text{Equation 8})$$

where $\psi_{\alpha i}$ is the alignment rule error and $\psi_{\beta i}$ is the cohesion rule error for boid i .

These errors are then multiplied by the rule weightings for alignment and cohesion, W_α and W_β , respectively, and summed to give the overall error. This error is then used to calculate the demanded load factor for the given boid:

$$n_i = 1 + \frac{1}{\pi} (W_\alpha \psi_{\alpha i} + W_\beta \psi_{\beta i}) \quad (\text{Equation 9})$$

or more explicitly

$$n_i = 1 + \frac{1}{\pi} (W_\alpha (\alpha - \psi_i) + W_\beta (\beta_i - \psi_i)) \quad (\text{Equation 10})$$

Note that if both rule weights are zero, or both heading angle errors are zero, equation 10 gives a load factor of 1, which corresponds to unaccelerated flight in a straight line, as required. Note also, that the $1/\pi$ scaling is used in equation 10 for reasons of convenience, i.e. for integer rule weightings, integer maximum load factors are obtained. For example, if $W_\alpha = W_\beta = 1$, a maximum load factor of 3 is achieved. In a practical application, the manoeuvrability of a given flight vehicle is normally defined by setting its maximum load factor. Following this, equation 10 can be used to define the maximum rule weights such that the maximum load factor is not exceeded.

The alignment angle, α , in equation 7 is calculated from the mean heading angle of the flock, equation 11.

$$\alpha = \frac{1}{m} \sum_{j=1}^m \psi_j \quad (\text{Equation 11})$$

This angle is common to all boids. The boid cohesion angle, β_i , in equation 8 is calculated from the angle of the cohesion vector, equation 12,

$$\beta_i = \arg(\mathbf{X}_q - \mathbf{X}_i) \quad (\text{Equation 12})$$

where

$$\mathbf{X}_q = \bar{\mathbf{X}} = \frac{1}{m} \sum_{j=1}^m \mathbf{X}_j \quad (\text{Equation 13})$$

and is specific to each boid.

Combining results (equations 10, 11, 12) and substituting into equation 1 yields equation 14. This equation gives the turn rate of boid i based on the positions and headings of the flock boids $j=1:m$ and the rule weightings W_α and W_β .

$$\dot{\psi}_i = \frac{g}{V_\infty} \sqrt{\left(\left(1 + \frac{1}{\pi} \left(W_\alpha \left(\left(\frac{1}{m} \sum_{j=1}^m \psi_j \right) - \psi_i \right) + W_\beta \left(\left(\arg \left(\left(\frac{1}{m} \sum_{j=1}^m \mathbf{X}_j \right) - \mathbf{X}_i \right) \right) - \psi_i \right) \right) \right)^2 - 1 \right)}$$

(Equation 14)

Whilst equation 14 (supplemented with equations 4 and 5) defines the motion of a single boid, it captures the essential dynamics of flocking, and its steady state solutions provide important insights into flocking behavior (Section D).

3. Flock scaling parameters

Within the flocking dynamics equation (equation 14) the flight vehicle cruise speed V_∞ is the only independent dimensional variable (g is constant). In mind of the need to produce results that can be generalized to flocking behavior of any flight vehicle, V_∞ is defined as the flock velocity scale. Following from this, a flock length scale, R_o , and a flock time scale, T_o , are defined as follows:

$$R_o = \frac{V_\infty^2}{g} \quad (\text{Equation 15})$$

$$T_o = \frac{V_\infty}{g} \quad (\text{Equation 16})$$

Following from equation 16, non-dimensional flock time is defined as

$$\tau = \frac{t}{T_o} \quad (\text{Equation 17})$$

where t is dimensional time.

Finally, as a further aid to data reduction, a non-dimensional flocking parameter, F , is defined as the ratio of the alignment and cohesion rule weights, equation 18.

$$F = \frac{W_\alpha}{W_\beta} \quad (\text{Equation 18})$$

4. Flock descriptors

The fundamental characteristics of flocking behavior can be captured in just two metrics, one describing the size of the flock based on the mean distance between flock members, and one describing the entropy of the flock based on the degree of alignment of the flock members. For the present work, the flock size is defined by the non-dimensional standard deviation of boid position and flock entropy by the non-dimensional standard deviation of boid velocity, equations 19 and 20, respectively. Note that flock size is normalized by the flock length scale and flock entropy normalized by the flock velocity scale.

$$\sigma_{\mathbf{x}} = \frac{1}{R_o} \left| \left(\frac{1}{m-1} \sum_{i=1}^m (\mathbf{X}_i - \bar{\mathbf{X}})^2 \right)^{\frac{1}{2}} \right| \quad (\text{Equation 19})$$

$$\sigma_v = \frac{1}{V_\infty} \left| \left(\frac{1}{m-1} \sum_{i=1}^m (\mathbf{V}_i - \bar{\mathbf{V}})^2 \right)^{\frac{1}{2}} \right| \quad (\text{Equation 20})$$

D. Analytical solution to the flocking dynamics equation: flocking modes

1. Overview

From preliminary numerical solution of equation 14 it was apparent that abrupt changes in flock behavior were obtained as the rule weightings were smoothly varied. This is consistent with critical phase change concepts derived from statistical physics studies described in the introduction (section I). Figure 5 illustrates the three predominant flocking phases, or modes, observed. When the cohesion rule dominates the alignment rule, boids orbit in either direction around a common center at a radius determined by the magnitude of cohesion rule weighting. This is defined as mode I. When the alignment rule dominates the cohesion rule, resulting behavior is characterized by strong velocity coherence, mode III. However, when the alignment and coherence rules have more equal weighting, the flock tends to exhibit chaotic behavior with low spatial and velocity coherence. This is defined as mode II. In the following, steady state solutions to the flocking equation (equation 14) are obtained and connections made with the flock modes described above.

2. Steady state unaccelerated motion

For steady state unaccelerated boid motion the load factor must be equal to 1. Setting $n_i = 0$ in equation 10 we obtain

$$W_\alpha (\alpha - \psi_i) + W_\beta (\beta_i - \psi_i) = 0 \quad (\text{Equation 21})$$

Trivial solutions of equation 21 are obtained for $W_\alpha = W_\beta = 0$ (non-flocking flight for all flocking schemes) and for $\psi_i = \alpha = \beta$ (flight along radii from the cohesion centroid for scheme B flocking). Non-trivial solution of equation 21 requires $W_\alpha > 0$, $W_\beta > 0$ and $\psi_i \neq \beta_i$. Rearranging equation 21 gives

$$\psi_i = \frac{W_\alpha \alpha + W_\beta \beta_i}{W_\alpha + W_\beta} \quad (\text{Equation 22})$$

If $W_\alpha \gg W_\beta$ i.e. $F \approx 1$, then $\psi_i \approx \alpha$ i.e. aligned flocking flight, defined as flocking mode III in figure 5.

For $W_\alpha \approx W_\beta$, i.e. $F \approx 1$, the heading angle for an individual boid is a weighted average of the boid cohesion angle and flock alignment angle. For a number of boids in a flock, the likelihood of achieving a steady state solution for this case is small, consistent with mode II chaotic motion.

3. Motion with constant acceleration

For steady state accelerated motion the load factor for each boid must be constant. Rearranging equation 10 we obtain

$$\psi_i = \frac{W_\alpha \alpha + W_\beta \beta_i - \pi (n_i - 1)}{W_\alpha + W_\beta} \quad (\text{Equation 23})$$

For the case of cohesion only, $W_\alpha = 0$, $W_\beta > 0$, equation 23 reduces to

$$\psi_i = \beta_i - \frac{\pi(n_i - 1)}{W_\beta} \quad (\text{Equation 24})$$

With reference to the geometry in figures 3 and 4, it can be deduced that for circular motion

$$\psi_i = \beta_i - \frac{\pi}{2} \quad (\text{Equation 25})$$

Thus, comparing equations 24 and 25 we obtain

$$\frac{\pi(n_i - 1)}{W_\beta} = \frac{\pi}{2} \quad (\text{Equation 26})$$

and hence

$$n_i = 1 + \frac{W_\beta}{2} \quad (\text{Equation 27})$$

Finally, substituting this value of n into equation 2 and non-dimensionalizing by the flock length scale, we obtain

$$r = \frac{1}{\sqrt{\frac{W_\beta^2}{2} + W_\beta}} \quad (\text{Equation 28})$$

Equation 28 indicates that as the cohesion rule strength W_β increases the non-dimensional radius of the circular flight path decreases, as would be expected.

Note that since alignment is zero, boids may travel round a circular path in different directions, consistent with flocking mode I in figure 5.

If both cohesion and alignment rules are applied, $W_a > 0$, $W_\beta > 0$, a steady state solution is obtained for scheme B flocking only, and this occurs when the alignment error is zero, i.e. $\alpha = \psi_i$. Substituting these values into equation 2 yields the same result as in equation 28 since the effect of W_a is cancelled; however in this case, the boids all orbit in the same direction. This is flocking mode III with a curved flight path.

III. Simulation framework

A flow diagram for numerical evaluation of the proposed flocking algorithm is shown in figure 6. The inner two loops perform the numerical integration of the flocking equations (equations 4, 5 and 14) for each boid over a time increment defined as the guidance interval. During this time, the load factors for each boid are constant. When the new positions of all the boids have been calculated, the flock centroids and boid load factors are calculated and a further integration sequence is performed. The procedure continues until a predefined stop time is reached, whereupon flock statistics are calculated for the accumulated results.

The numerical integration was performed using the variable time step Runge-Kutta ODE solver function within Matlab, with a default relative error tolerance of 1e-3. Note that for reasons of computational efficiency, the guidance interval was typically a number of orders of magnitude greater than the time step in the inner integration loop. The actual value of guidance interval used was determined from numerical experiments (see following section).

IV. Results

A. Determination of guidance time step

Experimentation showed that numerical accuracy of the flocking equations integration as a function of guidance time step was dominated by the magnitude of the alignment weighting, W_α . Figure 7 shows the effect of varying guidance interval on the non-dimensional time history of the flock entropy for $W_\alpha=4$. For this particular case, qualitative guidance time step independence was achieved for guidance intervals less than 0.05 (non-dimensional time). For lower values of W_α the guidance interval could be relaxed. For efficient implementation, a practical approach was adopted whereby the guidance interval was conservatively chosen to ensure time step independence for the particular value of W_α used for each simulation run.

B. Validation of flock scaling parameters

To validate the flock scaling parameters defined in section IIC3 a number of numerical experiments were performed. Figure 8 shows the time history of flock size for flocks of varying cruise velocity. The superposition of the results shows that flock scaling parameters are dimensionally sound. (Note that the flock dimensional starting size is multiplied by the flock length scale such that the non-dimensional start size is constant for all flocks.)

C. Numerical validation of analytical solution to flocking equations

In section IID3, it was shown that a constant acceleration steady state solution to the flocking equations was given by circular boid motion and the radius was a function of W_β only (equation 28). To validate this result, a scheme B flocking numerical experiment was performed investigating the effect of W_β on flock size, figure 9. The converged flock size at around $\tau = 50$ was then plotted as a function of W_β , figure 10. The converged flock size predicted analytically from equation 28 (noting that $\sigma_X = R$ for points distributed around a circle of non-dimensional radius R) is also shown for comparison, and excellent agreement is demonstrated. This provides evidence to support the validity of the numerical approach adopted.

D. Effect of flock population size

From numerical investigations, it was found that flock behavior was relatively insensitive to the number of boids in the flock for a population of 5 or more. For the present work, all evaluations were performed with a flock population size of 9.

E. Flocking rule weight space evaluation

To gain insight into the range of possible flock steady state behaviors for different rule weightings, flock steady state size and entropy was evaluated for each flocking scheme A, B and C over a 20x20 matrix of rule weights covering the space $0 < W_\alpha < 1$, $0 < W_\beta < 1$, figure 11. Note that some steady state solutions exhibit periodic variation in σ_X and σ_V . To accommodate this, the average of a number of cycles was calculated.

The first thing to notice from figure 11 is that contours of σ_X and σ_V are aligned with lines of constant F (where $F = W_\alpha / W_\beta$). This demonstrates that the flocking parameter F is a fundamental parameter determining flocking behavior.

The second important point is that the σ_X and σ_V results are qualitatively similar for all three flocking schemes. Following from the previous observation, this implies that the flocking parameter F controls flock behavior *independent of the flocking scheme*

used. Thus, F is the fundamental parameter controlling flocking behavior for the present flocking implementation.

To investigate the effect of F in more detail, a diagonal slice through the rule weight space was defined by the line $W_\beta = 1 - W_\alpha$. From this, 200 values of F between 0 and 5 were chosen randomly and steady state σ_X and σ_V obtained for scheme A flocking, figure 12. In figure 12a, the peak in σ_X around $F = 1.4$ corresponds to the dark area for the same F in figure 11a. Similarly in figure 12b, the peak in σ_V around $F = 1.4$ corresponds to the dark area for the same F in figure 11b. (Note however that when comparing figures 11a and b to figures 12a and b, F does not scale linearly with distance along the weight space slice in figure 11). To help understand the form of the above results, figure 13 shows an outline view of figure 12 with the F scale divided into zones defined by observed flocking mode. From this, it is clear that the abrupt changes in flock behavior with increasing F correspond to changes in the predominant flock mode.

F. Flock size and entropy time histories as a function of F

Time histories of σ_X and σ_V for scheme A flocking for varying values of F are shown in figure 14. For $F = 0$ ($W_\alpha = 0$, $W_\beta = 1$) the flock converges to mode I flocking after $\tau = 10$. Increasing F to 1.5 leads to mode II behavior. However, with $F = 2$, the flock initially exhibits mode II behavior then after $\tau = 20$, changes to mode III, reaching σ_X convergence at $\tau = 60$. Increasing F destabilizes the mode II and reduces the time taken to achieve mode III. The time to reach σ_X convergence is, however, increased.

As a further aid to visualization, selected cases from figure 14 are also shown as X-Y trajectories in figure 15. The plane symbols indicate the position and orientation of a given boid and for clarity only half the boids are shown.

Time histories of σ_X and σ_V for scheme B flocking are shown in figure 16, supported by trajectories in figure 17. The $F = 0$ case is nearly identical to scheme A flocking, as would be expected. For $F = 1.5$, oscillatory mode II behavior is exhibited with periodic variation in both σ_X and σ_V . Increasing F to 4 increases the stability of mode III and eventually after $\tau = 150$, converged mode III behavior is achieved.

V. Conclusions

1. Flight vehicle flocking behavior with high spatial and velocity coherence (mode III flocking) offers opportunities for safe operation of flight vehicles at very high traffic densities.
2. Three strategically relevant flocking schemes are identified. In scheme A, boids align to a predefined alignment vector. In scheme B, boids converge towards a predefined cohesion centroid. In scheme C there is no predefined alignment vector or cohesion centroid and boids operate as a free flock.
3. A simple 2D air vehicle flocking algorithm has been developed based on a constant speed, bank to turn aircraft model. The flocking algorithm is based on two rules: alignment and cohesion. These two rules are sufficient to generate useful flocking behavior.
4. The flocking model is non-dimensionalized such that the results can be scaled to vehicles of any given mass and flight speed.

5. Model dynamics are integrated between guidance events using a variable time step solver. The guidance interval for time step independence was strongly dependent on the alignment rule weighting, and was obtained a priori through numerical experimentation.
6. Flocking behavior is usefully described by the time evolution of two statistical parameters: the non-dimensional standard deviation of position (flock size) and the non-dimensional standard deviation of velocity (flock entropy).
7. The proposed flocking rules generate heading angle guidance information for a given boid based on the boid's position and velocity, and the global cohesion and alignment centroids for the flock. Load factor is then scaled on the heading angle errors for each rule according the rule weights.
8. Steady state analytical solution of the differential equations governing the present flocking algorithm indicate the existence of a number of flocking modes. The existence of these modes has been validated through numerical evaluation of the flocking model.
9. The type of flocking behavior obtained (i.e. flock mode) is determined by a simple flocking parameter F based on the ratio of alignment to cohesion rule weight. This parameter controls flocking mode independent of the flocking scheme employed.
10. The first flocking mode occurs for $F < 1$ and is based on circular motion about a common center but with no predefined direction of rotation. The second mode is chaotic and occurs for $F \approx 1.4$. The third mode occurs for $F > 2$ and generates strategically useful boid motion with high spatial and velocity coherence.

VI. Further Work

In the present work, the flock is fully homogenous in that the same rules and rule weights apply to each boid and each boid has identical sensors. Current research into multi-agent systems suggests that the overall system fitness can be improved by giving agents non-homogenous behaviors. For example, it may be advantageous to provide a distribution of rule weightings across the flock. Similarly, it may be beneficial to distribute different sensors amongst the flock; giving some boids sensors optimized for long range with narrow field of view and others short range with wide field of view. Following from this, in relation to practical application of the work, it is also necessary to investigate the effect of non-ideal sensor behavior, i.e. limited resolution and accuracy.

References

1. *Free Flight Implementation*, Final Report of Radio Technical committee on Aeronautics (RTCA), Task Force 3, RTCA, Inc., Washington, DC, Oct. 1995.
2. Byrne, G., "Is it time to give airliners the freedom of the skies?" *New Scientist* Vol. 175 issue 2351 - 13 July 2002, page 12
3. Paielli, R. A., and Erzberger, H., "Conflict probability estimation for free flight," *Journal of Guidance, Control and dynamics*, Vol. 20., No. 3, 1997, pp. 588-596.
4. Zegaha, K., "A Review of Different Approaches Based on Force Fields for Airborne Conflict Resolution," AIAA Paper 98-4240, Aug. 1998.
5. Miura, A., Morikawa, H., and Mizumachi, M., "Aircraft Collision Avoidance with Potential Gradients – Ground-Based Avoidance for Horizontal Maneuvers," *Electronics and Communications in Japan*, Pt. 3, Vol. 78., No. 10, 1995, pp. 104-114.
6. Burdun, I. and Parfentyev, O., "AI knowledge model for self-organizing conflict prevention/resolution in close free-flight air space", IEEE Aerospace Applications Conference Proceedings, Vol. 2, 1999, pp. 409-428.
7. Gabbai, J.M., Wright, W.A. and Allinson, N.M., "Relating organisational structure to performance: an initial focus on centralisation", Net.Object Days Conference, October 2002.
8. Gueron, S.A., Levin, S., Rubenstein, D.I., "The dynamics of herds: from individuals to aggression", *Journal of Theoretical Biology*, Vol.182, 1996, pp. 85-98
9. Potts, W., "The chorus line hypothesis of manoeuvre coordination in avian flocks", letter in *Nature*, Vol. 309, May 24, 1984, pp. 344-345.
10. Shaw, E., "Fish in schools", *Natural History* 84, No. 8, 1975, p. 4046
11. Partridge, B., "The structure and function of fish schools", *Scientific American*, June 1982, pp. 114-123.
12. Wright, W.A., Smith, R.E., Danek, M. and Greenway, P., "A measure of emergence in an adapting, multi-agent context", presented at SAB 2000, Paris, 2000.
13. Pachter, M., D'azzo, J. J., and Dargan, J. L., "Automatic Formation Flight Control," *Journal of Guidance, Control and Dynamics*, Vol. 17, No. 6, 1994.
14. Blake, W., and Multhropp, D., "Design, Performance and Modeling Considerations For Close Formation Flight," *AIAA Guidance, Navigation and Control Conference*, AIAA, Reston, VA, July 1998.
15. Anderson, M., Robbins, A., "Formation flight as a cooperative game", AIAA Guidance, Navigation and Control Conference and Exhibit, Boston, MA, August 1998, Technical Papers pt 1 (A98-37001 10-63), pp. 244-251.
16. Wang, P. K. C., and Hadaegh, F. Y., "Coordination and control of Multiple Microspacecraft Moving in Formation," *Journal of Astronautical Sciences*, Vol. 44, No. 3, 1996, pp. 315-355.
17. Reynolds, C., "Flocks, Herds, and Schools: a distributed behavioral model", *Computer graphics*, 21(4), July 1987, pp. 25-34.
18. Shimoyama, N., Sugawara, K., Mizuguchi, T., Hayakawa, Y., and Sano, M., "Collective motion in a system of motile elements", *Physical Review Letters*, 1996, Vol. 76, No. 20, pp. 3870-3873.
19. Vicsek, E., Shochet, I., "Novel types of phase transition in a system of self-driven particles", *Physical Review Letters*, Vol. 75(6), 1995, pp. 1226-1229.

20. Toner, J., Tu, Y., "Flocks, herds, and schools: A quantitative theory of flocking", *Physical Review E*, Vol. 58, No. 4, October 1998, pp. 4828-4858.
21. Czirok, A., Vicsek, M., Vicsek, T., "Collective motion of organisms in three dimensions", *Physica A*, Vol. 264, No. 1-2, Feb. 1999, pp. 299-304.
22. Crowther, W.J. and Riviere, X., "Flocking of unmanned air vehicles", 17th UAV Systems Conference, Bristol, UK, April 2002.
23. Hwang, Y., and Ahuja, N., "A potential Field Approach to Path Planning," *IEEE Transactions of Robotics and Automation*, Vol. 8, No. 1, 1992, pp. 23-32.
24. Frazzoli, E., Dahleh, M. A., and Feron, E., "Real-time motion planning for agile autonomous vehicles," *Journal of Guidance, Control and Dynamics*, Vol. 25, No. 1, 2002, pp. 116-129.
25. Anderson, J. D., *Introduction to flight*, fourth edition, McGraw-Hill, Chapter 6, p. 430.

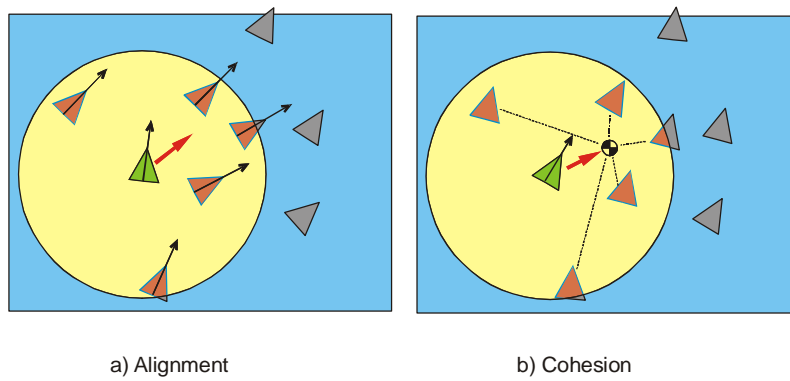


Figure 1 Schematic representation of the alignment and cohesion rules for

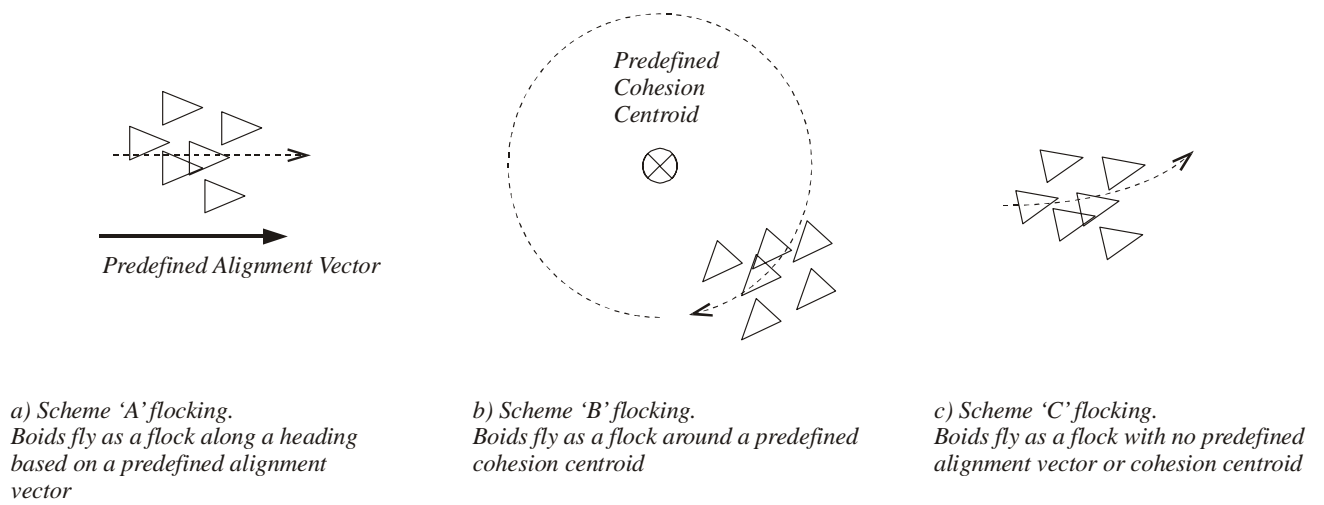


Figure 2 Definition of three different flocking

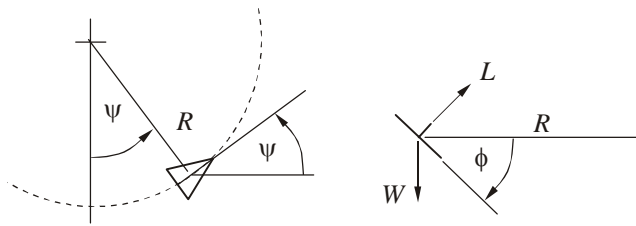


Figure 3 Aircraft performing a steady, banked turn in the horizontal plane.

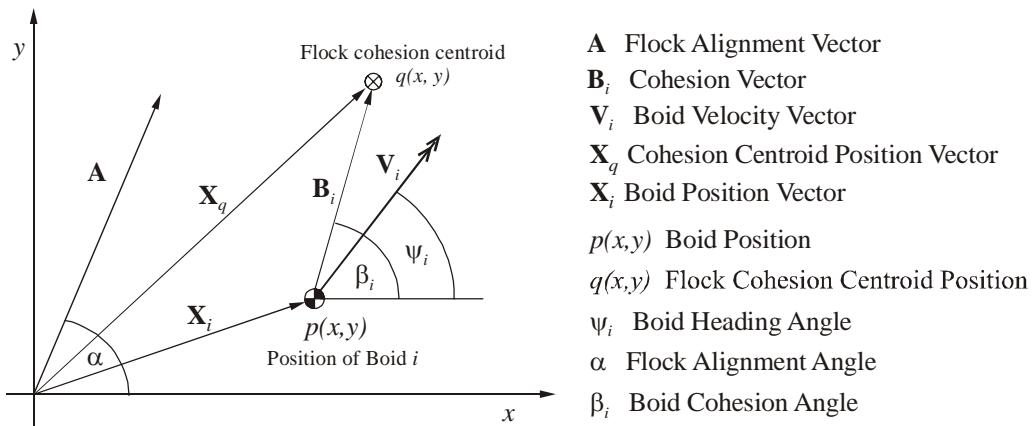


Figure 4 Angle, position and vector definitions for a flocking boid.

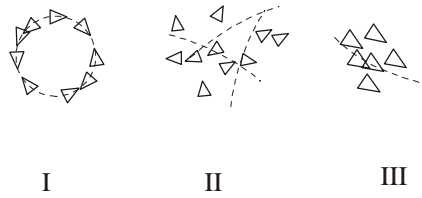


Figure 5 Schematic of the three fundamental flocking modes.

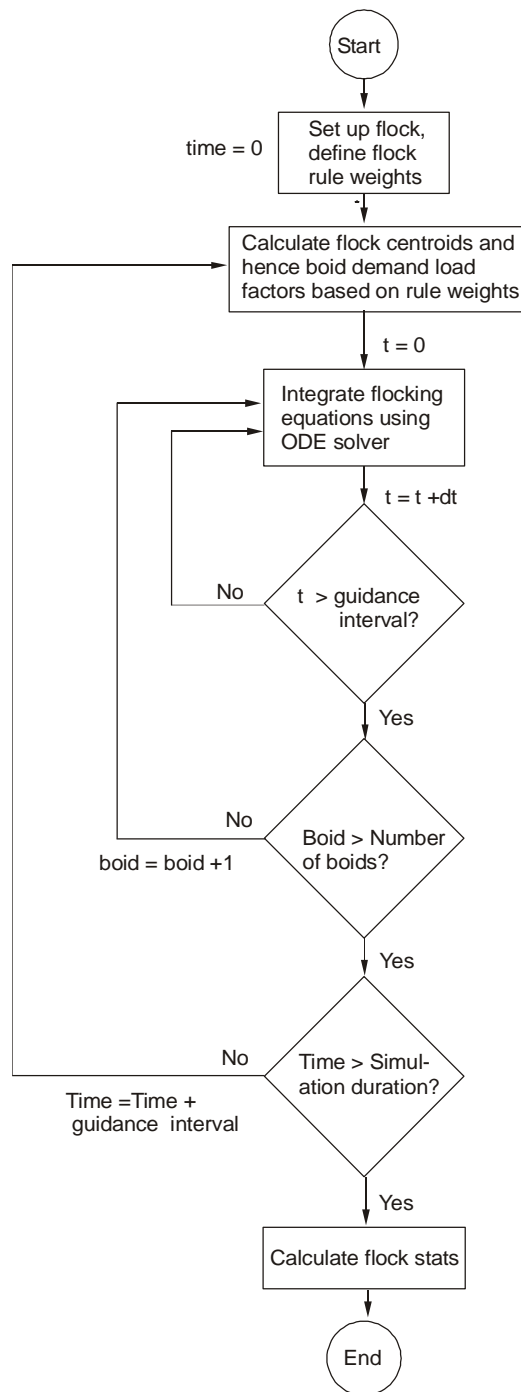


Figure 6 Logic flow diagram for flocking algorithm implementation.

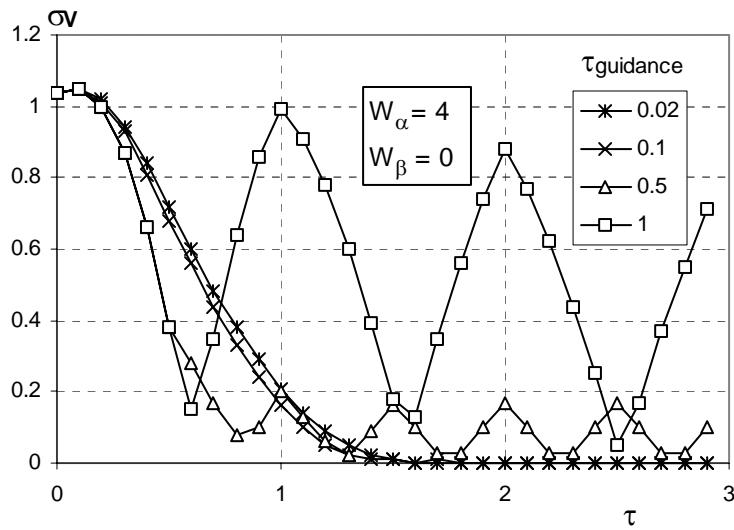


Figure 7 Effect of guidance interval on flock entropy time history for an alignment weighting of 4, cohesion weighting = 0, scheme A flocking. Guidance interval independence is achieved for $\tau_{\text{guidance}} < 0.1$.

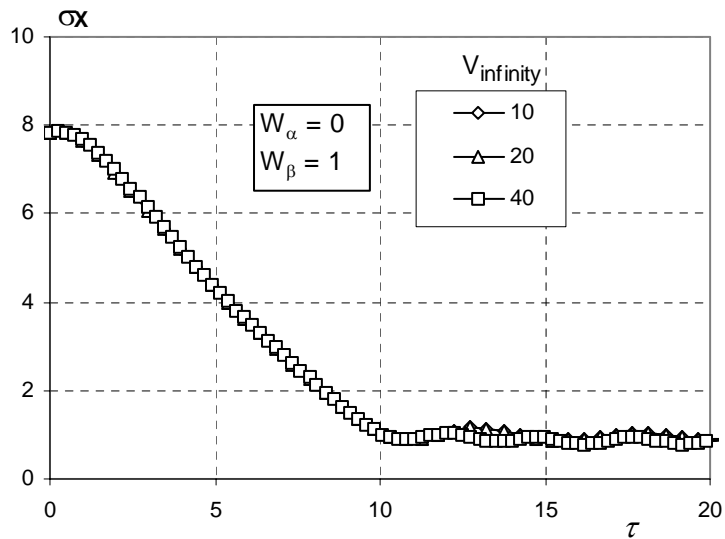


Figure 8 Flock size time histories for varying cruise speed, fixed rule weightings, scheme B flocking. The collapse of the data demonstrates validity of the velocity scaling used.

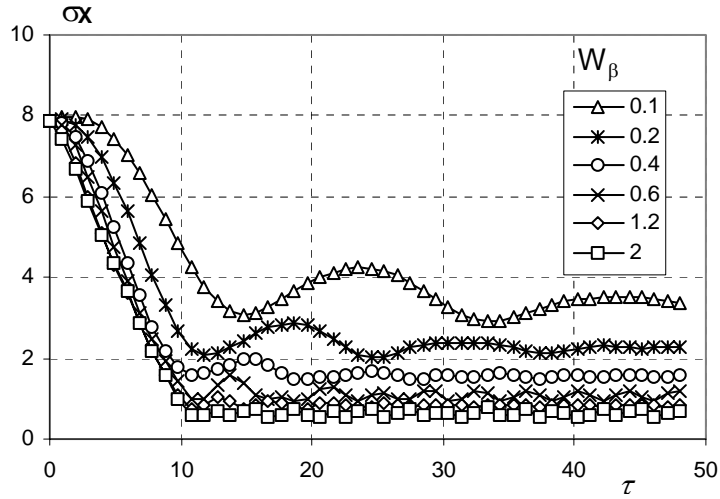


Figure 9 Flock size time histories for varying cohesion rule weight, scheme B flocking.

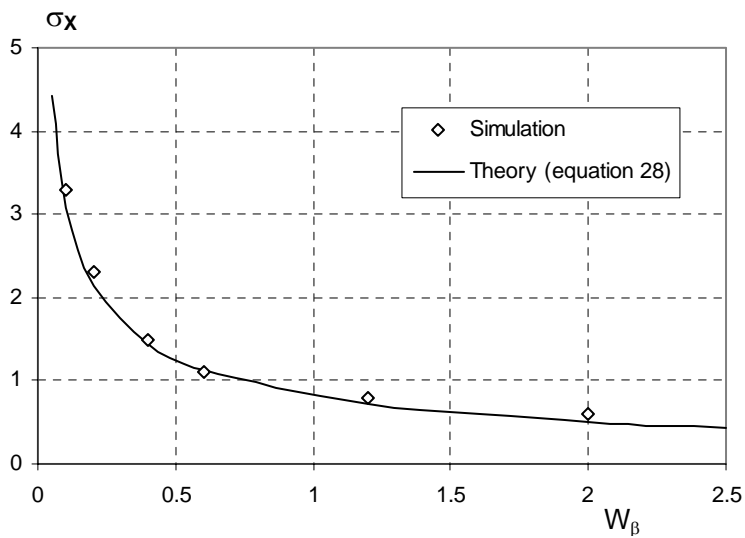


Figure 10 Steady state flock size as a function of cohesion rule weighting, scheme B flocking. A strong correlation between numerical and analytical results is demonstrated.

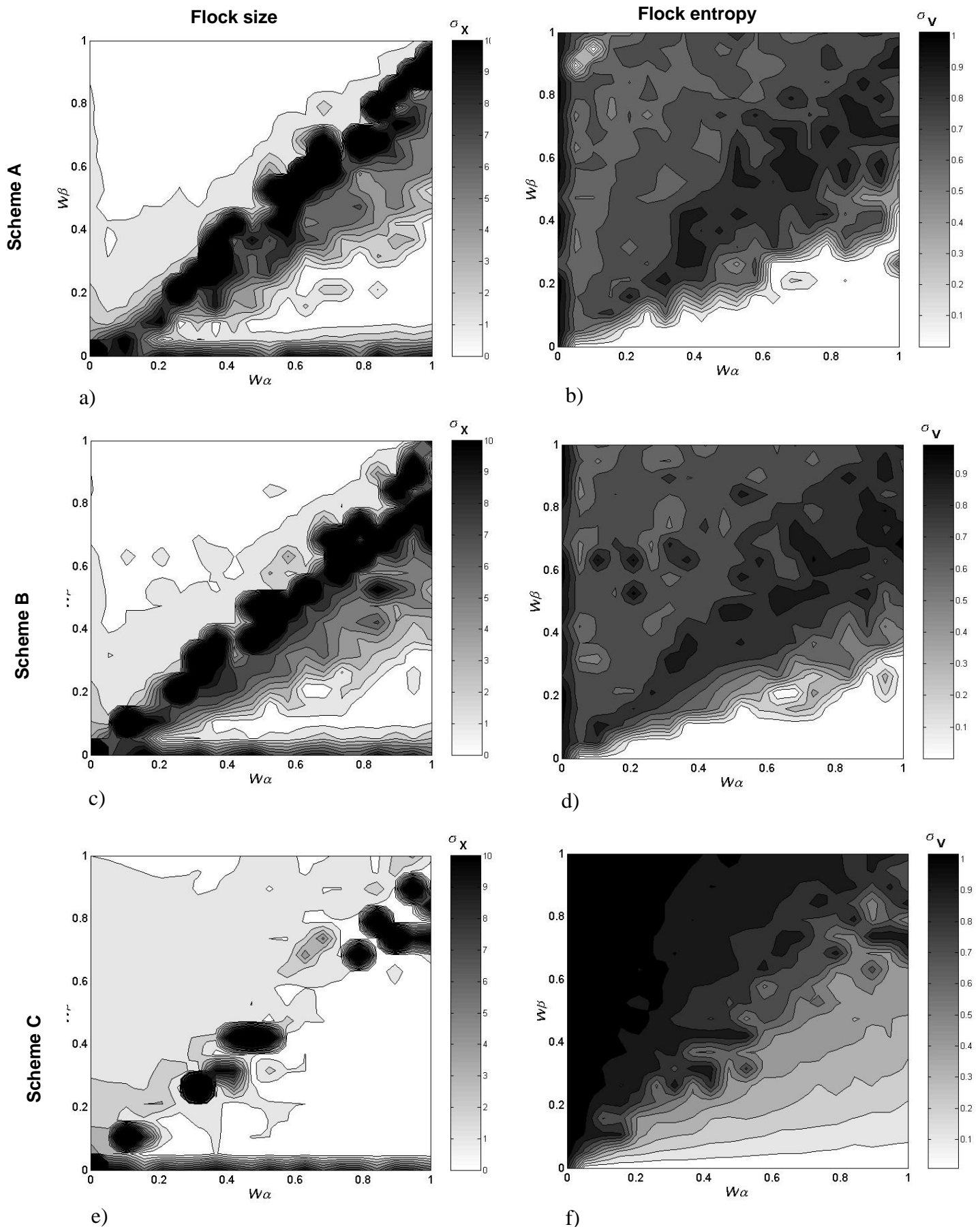


Figure 11 Steady state flock size and flock entropy contours as a function of alignment and cohesion rule weights for flocking schemes A, B and C. Note that all three flocking schemes show qualitatively similar results. From this figure it can be concluded that the ratio of alignment to cohesion rule weights is the fundamental parameter determining flocking steady state behaviour.

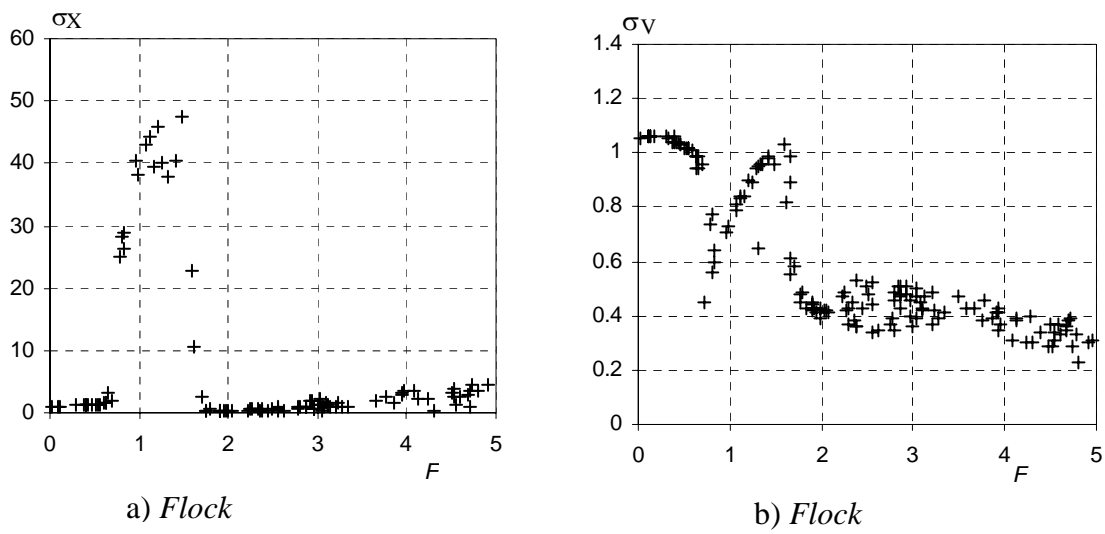


Figure 12 Steady state flock size and entropy as a function of the ratio of alignment to cohesion rule weights, scheme A flocking.

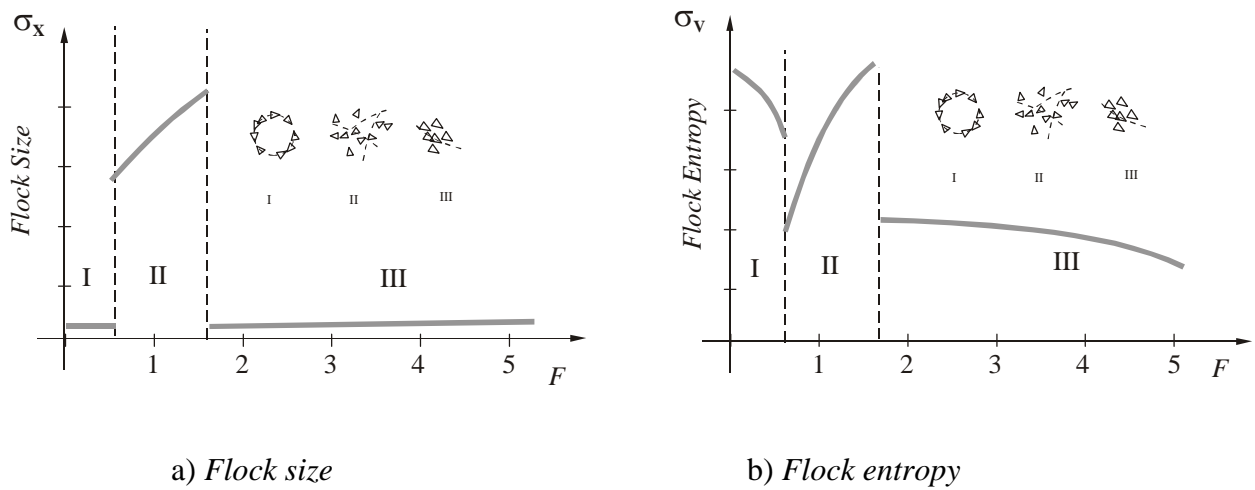


Figure 13 Schematic representation of figure 12 correlating flock modes with different flocking parameter zones.

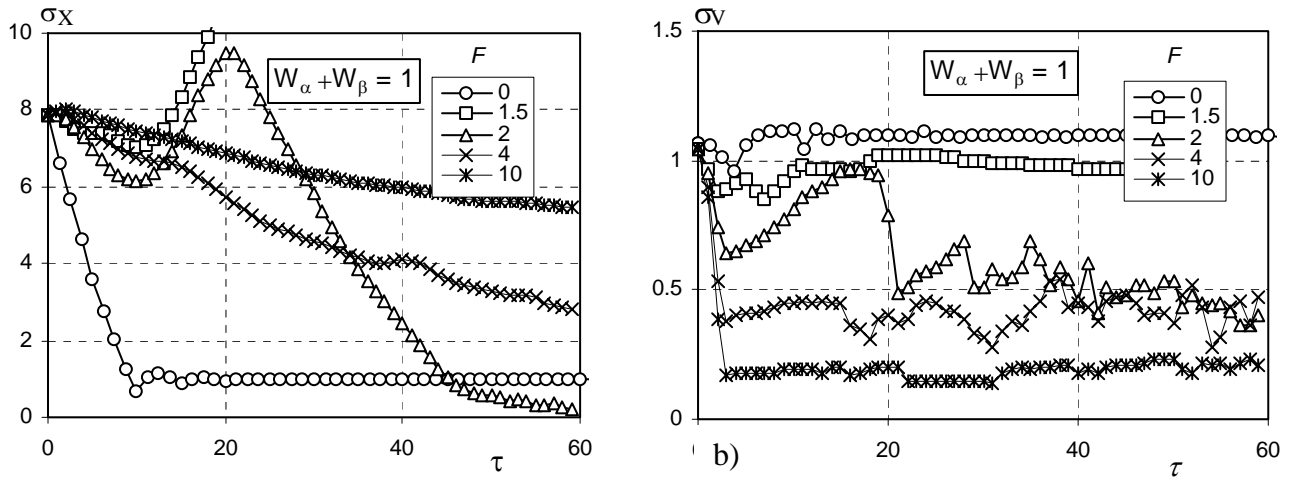


Figure 14 Flock size and entropy time histories for varying flocking parameter, scheme A flocking.

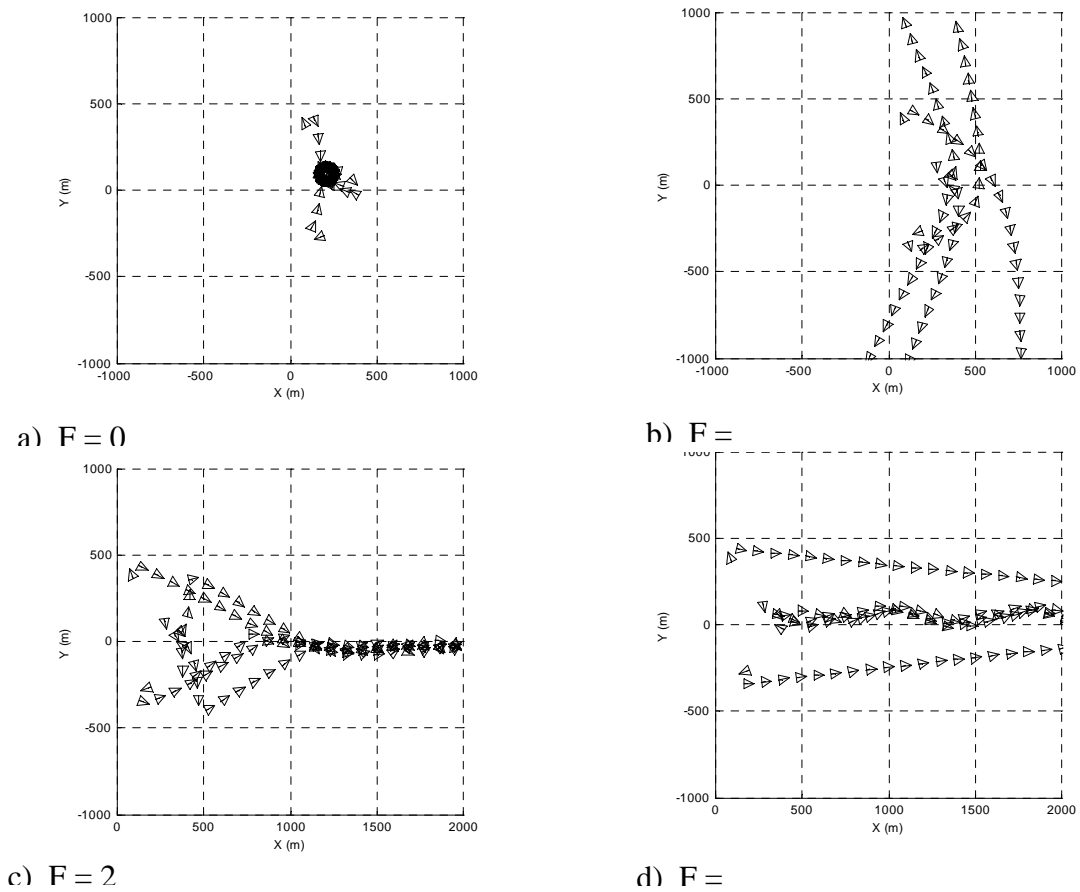


Figure 15 Boid trajectories for varying values of flocking parameter, scheme A flocking.

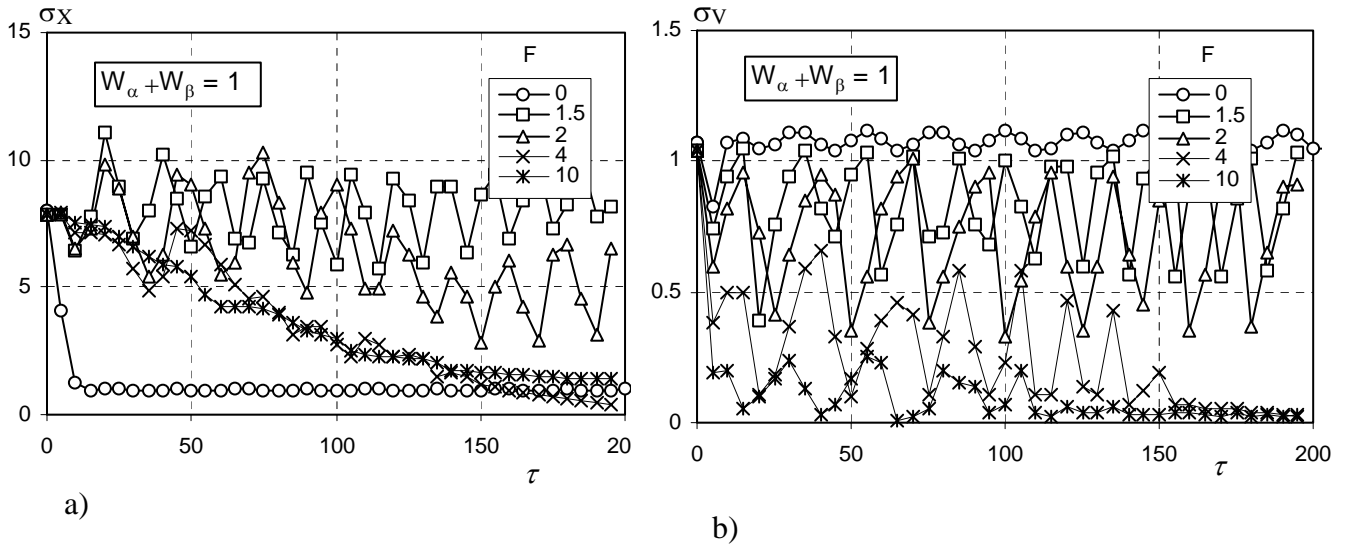


Figure 16 Flock size and entropy time histories for varying flocking parameter, scheme B flocking.

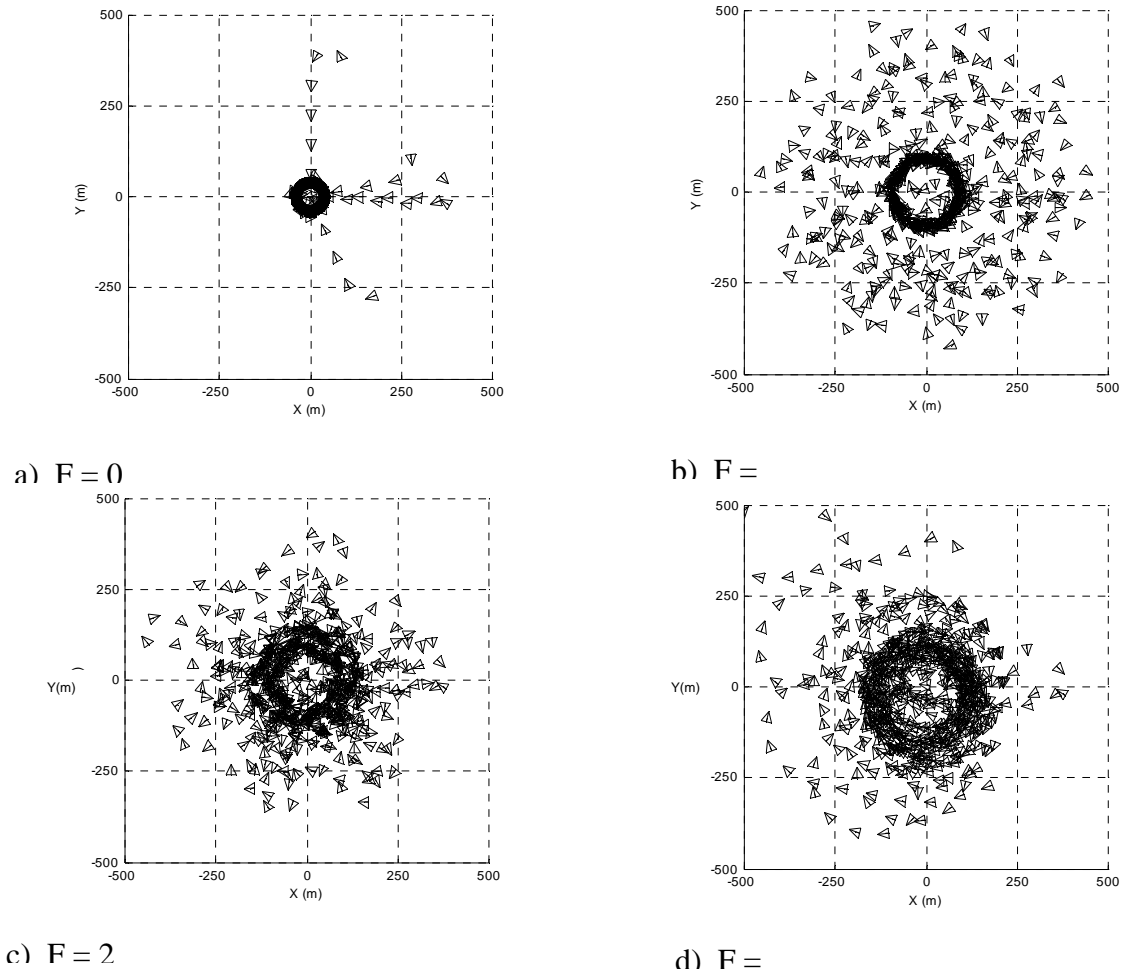


Figure 17 Boid trajectories for varying values of flocking parameter, scheme B flocking.